Title
Microbiome-metabolomics reveals gut microbiota associated with glycine-conjugated metabolites and polyamine metabolism in chronic kidney disease.

Journal
Cellular and molecular life sciences : CMLS, 76(24)

ISSN
1420-682X

Authors
Feng, Ya-Long
Cao, Gang
Chen, Dan-Qian
et al.

Publication Date
2019-12-01

DOI
10.1007/s00018-019-03155-9

Peer reviewed

Cellular and Molecular Life Sciences
https://doi.org/10.1007/s00018-019-03155-9

ORIGINAL ARTICLE

Microbiome–metabolomics reveals gut microbiota associated with glycine-conjugated metabolites and polyamine metabolism in chronic kidney disease

Ya-Long Feng[1] · Gang Cao[3] · Dan-Qian Chen[1] · Nosratola D. Vaziri[2] · Lin Chen[1] · Jun Zhang[1] · Ming Wang[1] · Yan Guo[4] · Ying-Yong Zhao[1]

Received: 28 February 2019 / Revised: 28 April 2019 / Accepted: 16 May 2019

Abstract

Dysbiosis of the gut microbiome and related metabolites in chronic kidney disease (CKD) have been intimately associated with the prevalence of cardiovascular diseases. Unfortunately, thus far, there is a paucity of sufficient knowledge of gut microbiome and related metabolites on CKD progression partly due to the severely limited investigations. Using a 5/6 nephrectomized (NX) rat model, we carried out 16S rRNA sequence and untargeted metabolomic analyses to explore the relationship between colon's microbiota and serum metabolites. Marked decline in microbial diversity and richness was accompanied by significant changes in 291 serum metabolites, which were mediated by altered enzymatic activities and dysregulations of lipids, amino acids, bile acids and polyamines metabolisms. Interestingly, CCr was directly associated with some microbial genera and polyamine metabolism. However, SBP was directly related to certain microbial genera and glycine-conjugated metabolites in CKD rats. Administration of poricoic acid A (PAA) and *Poria cocos* (PC) ameliorated microbial dysbiosis as well as attenuated hypertension and renal fibrosis. In addition, treatments with PAA and PC lowered serum levels of microbial-derived products including glycine-conjugated compounds and polyamine metabolites. Collectively, the present study confirmed the CKD-associated gut microbial dysbiosis and identified a novel dietary and therapeutic strategy to improve the gut microbial dysbiosis and the associated metabolomic disorders and retarded the progression of kidney disease in the rat model of CKD.

Keywords Renal fibrosis · Gut microbiota · Metabolome · Hypertension · Creatinine clearance rate · Polyamine metabolism

Introduction

Chronic kidney disease (CKD) has emerged as a major public health problem with increased morbidity and mortality. Patients with CKD are at increased risk for the development of cardiovascular disease (CVD) beyond traditional risk factors [1]. Angiotensin-converting enzyme inhibitors and angiotensin receptor blockers are identified as the first-line therapies that proved efficient to retard the progression of hypertension, CVD and CKD [2]. Nevertheless, although this approach is undoubtedly effective, many CKD patients who are treated with these drugs progress to end-stage renal disease (ESRD), underscoring the importance of novel therapeutics on disease intervention.

The human gut is heavily populated with myriad microorganisms. The normal gut microbial community forms a natural defense barrier and favorably influences the hosts' physiology, immune function, nutrition, inflammatory signaling

Ya-Long Feng, Gang Cao and Dan-Qian Chen contributed equally as co-first authors to this work.

Electronic supplementary material The online version of this article (https://doi.org/10.1007/s00018-019-03155-9) contains supplementary material, which is available to authorized users.

✉ Ying-Yong Zhao
zyy@nwu.edu.cn; zhaoyybr@163.com

1 School of Pharmacy, Faculty of Life Science & Medicine, Northwest University, No. 229 Taibai North Road, Xi'an, Shaanxi 710069, China

2 Division of Nephrology and Hypertension, School of Medicine, University of California Irvine, Irvine, CA 92897, USA

3 School of Pharmacy, Zhejiang Chinese Medical University, No. 548 Binwen Road, Hangzhou, Zhejiang 310053, China

4 Department of Internal Medicine, Comprehensive Cancer Center, University of New Mexico, Albuquerque, NM 87131, USA

Published online: 30 May 2019

and metabolisms of lipids, bile acids, indole, choline, short-chain fatty acids, etc. [3, 4]. Among them, the levels of low-molecular-weight metabolites are closely associated with the composition of the gut microbiota. Metabolites derived from the gut's bacteria provide an insight into the metabolic state of an individual [5]. Various clinical and animal studies have demonstrated the critical role of the gut microbiota in both health maintenance and disease pathogenesis [3, 4]. Under normal conditions, there is equilibrium between the intestinal bacteria and the host, via the innate immunity that maintains the balance of inflammation and intestinal barrier integrity. However, by altering the biochemical and biophysical milieu of the intestinal tract, advanced CKD results in intestinal epithelial barrier disruption and microbial dysbiosis [6]. Recent studies have illuminated the effect of CKD on the gut microbiota pointing to the kidney–gut axis [7]. CKD has been shown to result in the dysbiosis of the gut microbiota, leading to an increased production of various uremic toxins including indoxyl sulfate (IS), p-cresyl sulfate (p-CS), trimethylamine and trimethylamine N-oxide (TMAO) [7] which accelerate the progression of CKD to ESRD by intensifying inflammation [8].

A deeper understanding of the gut microbiome–metabolome axis is a prerequisite to improve therapeutic strategies that manipulate the gut microbiota in the course of development of CKD. It has been reported that patients with ESRD have expansion of *Firmicutes*, *Actinobacteria* and *Proteobacteria* phyla and reduction of *Bifidobacteria* and *Lactobacilli* populations in their colons [9]. Several studies have also uncovered marked alteration of the microbiota composition in hemodialysis patients [10]. Alterations in microbiome composition results in increased generation of lipopolysaccharide, IS, p-CS, amines and ammonia that lead to the activation of proinflammatory cytokine/chemokine cascades in CKD and ESRD [11]. Elevation of IS and p-PC levels may accelerate the progression of CKD and the CKD-associated cardiovascular diseases [12]. In fact, a series of clinical studies have demonstrated the association of increased IS and p-CS levels with the progression and mortality of renal diseases in CKD/ESRD populations [8]. Moreover, elevated IS and p-CS levels were implicated in high levels of inflammatory markers in patients with CKD and played pivotal roles in the prediction of CKD progression [13]. The relationship between fasting serum TMAO and all-cause mortality over a 5-year follow-up were examined in 521 subjects with stable CKD. Serum TMAO levels were significantly increased, which was closely involved in poor long-term survival in CKD patients and progressive renal fibrosis in CKD animals [14].

Heretofore, few studies have been assigned to explore the direct association between gut microbiome and serum metabolites in CKD [8]. Several important gaps in knowledge of gut microbiota and endogenous metabolites remain unexplored and deeper investigations are urgently needed. To this end, we first applied 16S rDNA sequencing technique and untargeted metabolomics to determine the effect of CKD on the gut microbiome and serum metabolites in rats with CKD induced by 5/6 nephrectomy (NX). In addition, an independent experiment was performed to verify the identified microbiota and metabolites as well as discover new intervention strategy on gut microbiota, hypertension and renal fibrosis in CKD.

Materials and methods

Experimental animals

Male Sprague–Dawley rats (180–200 g) were purchased from the Central Animal Breeding House of Xi'an Jiaotong University (Xi'an, Shaanxi, China). Animal protocols were approved by Northwest University institutional animal care and use committee (Permit Number: SYXK 2010-004). The rats ($n=12$) were randomized into two groups: sham and NX groups. The NX were performed as previously described [15]. Briefly, the 2/3 of the left kidney and the whole right kidney were removed by scalpel excision. Gelfoam coagulant was further applied on the cut surfaces. The Sham were merely subjected to laparotomy. To verify the identified microbiota and metabolites as well as discover new intervention strategy, a separate experiment was performed. CKD rats were treated with *Poria cocos* (PC, a well-known medicinal compound derived from fungal mushroom) and poricoic acid A (PAA, a tetracyclic triterpenoid compound isolated from PC) or placebo. They were randomized into four groups ($n=8$/group): sham, NX, NX + PAA and NX + PC. The ethanol-extracted PC (250 mg/kg/day) and PAA (10 mg/kg/day) were gavaged into NX rats. All animals were provided access to water and food ad libitum. The sham-operated, NX and treated rats were sacrificed at week 12. Blood, colonic luminal contents, colon tissues and kidney tissues were collected and processed for 16S rRNA sequence, untargeted and targeted metabolomic, histological and western blot analyses.

Renal function and blood pressure

Serum creatinine, urea and proteinuria were measured by Olympus AU6402 automatic analyzer. Additionally, creatinine clearance rate (CCr) was calculated on the basis of relevant data and a weekly measurement of blood pressure was performed by rat tail plethysmograph as well(Techman Soft, Chengdu, China).

Histological analysis

Glomerulosclerosis and tubulointerstitial damage were assessed by periodic acid–Schiff (PAS) staining and Masson's trichrome staining as previously described [16]. Immunohistochemistry (IHC) procedure was carried out as previously described [17]. The histological assessments were performed by two independent pathologists. After immunohistochemical analysis, Image-Pro plus software version 6.0 was used to analyze the optical density of the images as described previously [17, 18].

Western blot analyses

The primary antibodies including ZO1, occludin, claudin-1, IκBα, p-IκBα, NF-κB p65, monocyte chemotactic protein-1 (MCP-1), cyclooxygenase-2 (COX-2), Keap1, Nrf2, heme oxygenase 1 (HO-1), catalase, NAD(P)H quinone dehydrogenase 1 (NQO1), α smooth muscle actin (α-SMA), collagen I and fibronectin were purchased from Abcam and Santa Cruz Companies. Colon and kidney tissues were processed for western blot analyses as previously described [19, 20]. Blots were processed with ECL reagent and protein concentrations were normalized against α-tubulin expression.

High-throughput sequencing of colon lumen DNA

The colon lumen of each sample was stored at − 80 °C for DNA extraction and dissected with sterilized blade. Genomic DNA was extracted using a E.Z.N.A.® Soil DNA Kit (Omega Bio-tek, Norcross, GA, USA) according to manufacturer's protocols. The concentrations and purity of the resultant DNA were determined by a NanoDrop (NanoDrop ND-2000, USA), which was stored at − 80 °C for further analysis.

The 16S rRNA gene was amplified by PCR with primers 16s-F (5′-AGAGTTTGATYMTGGCTCAG-3′) and 16s-R (5′-TGCTGCCTCCCG TAGGAGT-3′) targeting the hypervariable V4–V5 region of the 16S rRNA gene of bacteria. PCR reactions were performed in triplicates with Phusion® High-Fidelity PCR Master Mix (New England Biolabs) using 10 ng template DNA. PCR products were purified using the AxyPrep DNA Gel Extraction Kit (Axygen Biosciences, Union City, CA, USA) according to the manufacturer's instructions and quantified using QuantiFluor™-ST (Promega, USA). The PCR products of different samples were mixed equally and subsequently used to construct Illumina Pair-End library using Next® Ultra™ DNA Library Prep Kit for Illumina (NEB, USA). Then, the amplicon library was paired end sequenced (2 × 250) on an Illumina HiSeq 2500 platform (Illumina, SanDiego, USA) according to the standard protocols.

Processing of 16S rRNA gene sequences

Raw fastq files were demultiplexed using the barcode sequence with the exact barcode matching parameter. Quality filtering was done using Trimmomatic (version 0.36) [21] with the following criteria: (1) bases off the start and end of a read below a threshold quality (score < 3) were removed, (2) the reads were truncated at any site receiving an average quality score < 5 over a 4-bp sliding window, discarding the truncated reads that were shorter than 100 bp. Paired reads were merged using USEARCH fastq_merge pairs command (version 9.2.64, http://drive5.com/uparse/) [22] with the default parameters. Operational units (OTUs) were clustered with 97% similarity cutoff using USEARCH UPARSE [23]. The chimeric sequences were removed in the UPARSE pipeline. The phylogenetic affiliation of each 16S rRNA gene sequence was analyzed by USEARCH SINTAX algorithm [24] against the RDP training set (version v16) 16S rRNA database using confidence threshold of 0.8. The OTUs identified as mitochondrial or chloroplast rRNA sequences were discarded. The rarefaction analysis based on USEARCH α_divisity [25] was conducted to reveal the diversity indices, including the richness, chao1, Simpson and Shannon diversity indices. The β diversity analysis was performed using UniFrac metrics [26] in QIIME (version 1.9.1) [27] pipeline.

Sample preparation and UPLC–MS analysis for metabolomics

Serum metabolites were performed using an untargeted metabolomics UPLC–HDMS. The metabolomic procedure, including sample preparation, metabolite separation and detection, data preprocessing and statistical analysis for metabolite identification, was performed following our previous protocols with minor modifications [28–31].

Statistics analysis

The statistical analyses were performed using R 2.15.0 and GraphPad Prism software v 5.0. PCA and OPLS-DA were performed using SIMCA-P software to cluster the sample plots across groups. All the data were presented as mean ± SEM. The significance of the difference between two groups was analyzed using Student's unpaired *t* test, and multiple comparisons were analyzed using one-way ANOVA followed by Dunnett's post hoc test. Differential abundances of genera and metabolites were determined by non-parametric tests including Wilcoxon rank sum test and Mann–Whitney *U* test. Serum metabolite intensities were then tested for association with 16S levels using Spearman rank correlation. *P* values were corrected for multiple

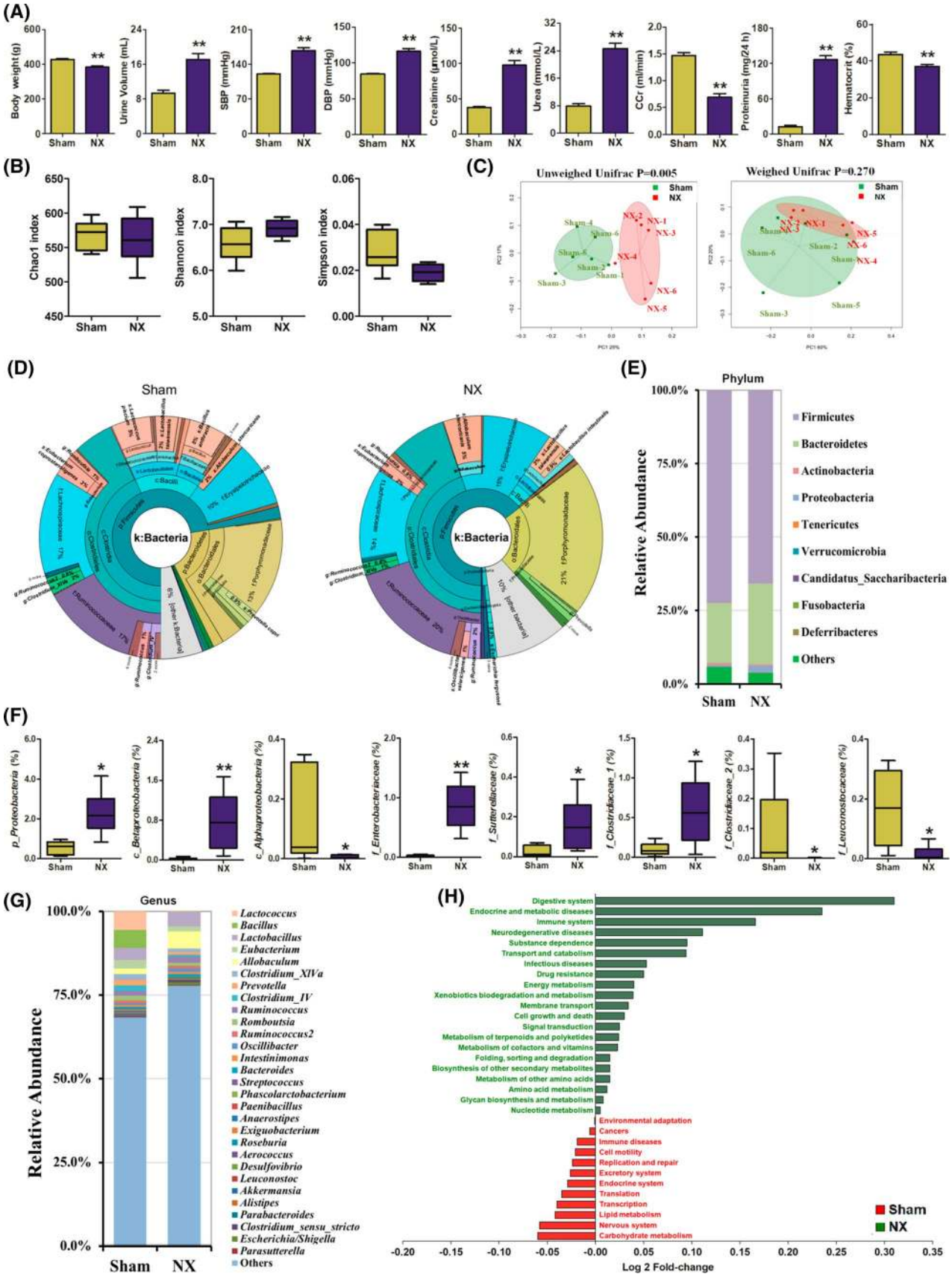
(A)
Body weight (g)
Urine Volume (mL)
SBP (mmHg)
DBP (mmHg)
Creatinine (μmol/L)
Urea (mmol/L)
CCr (ml/min)
Proteinuria (mg/24 h)
Hematocrit (%)
Sham
NX
(B)
Chao1 index
Shannon index
Simpson index
(C)
Unweighed Unifrac P=0.005
Weighed Unifrac P=0.270
(D)
Sham
NX
k:Bacteria
(E)
Phylum
Relative Abundance
Firmicutes
Bacteroidetes
Actinobacteria
Proteobacteria
Tenericutes
Verrucomicrobia
Candidatus_Saccharibacteria
Fusobacteria
Deferribacteres
Others
(F)
p_Proteobacteria (%)
c_Betaproteobacteria (%)
c_Alphaproteobacteria (%)
f_Enterobacteriaceae (%)
f_Sutterellaceae (%)
f_Clostridiaceae_1 (%)
f_Clostridiaceae_2 (%)
f_Leuconostocaceae (%)
(G)
Genus
Relative Abundance
Lactococcus
Bacillus
Lactobacillus
Eubacterium
Allobaculum
Clostridium_XlVa
Prevotella
Clostridium_IV
Ruminococcus
Romboutsia
Ruminococcus2
Oscillibacter
Intestinimonas
Bacteroides
Streptococcus
Phascolarctobacterium
Paenibacillus
Anaerostipes
Exiguobacterium
Roseburia
Aerococcus
Desulfovibrio
Leuconostoc
Akkermansia
Alistipes
Parabacteroides
Clostridium_sensu_stricto
Escherichia/Shigella
Parasutterella
Others
(H)
Digestive system
Endocrine and metabolic diseases
Immune system
Neurodegenerative diseases
Substance dependence
Transport and catabolism
Infectious diseases
Drug resistance
Energy metabolism
Xenobiotics biodegradation and metabolism
Membrane transport
Cell growth and death
Signal transduction
Metabolism of terpenoids and polyketides
Metabolism of cofactors and vitamins
Folding, sorting and degradation
Biosynthesis of other secondary metabolites
Metabolism of other amino acids
Amino acid metabolism
Glycan biosynthesis and metabolism
Nucleotide metabolism
Environmental adaptation
Cancers
Immune diseases
Cell motility
Replication and repair
Excretory system
Endocrine system
Translation
Transcription
Lipid metabolism
Nervous system
Carbohydrate metabolism
Sham
NX
Log 2 Fold-change

◂**Fig. 1** The alteration of gut microbiome in CKD rats. **a** Physiological and biochemical parameters of sham and NX rats. $^{**}P<0.01$ versus sham rats. **b** The α-diversity indexes of Chao1, Shannon and Simpson of gut microbiota between NX and sham rats. **c** Principal coordinate analyses based on unweighted and weighted (right) UniFrac distances between gut bacterial communities of NX and sham rats. *P* value indicated differential clustering assessed by ADONIS test. **d** The cladogram of different abundant taxa between samples from sham and NX rats using phylum- to genus-level data. **e** Taxonomic distributions of bacteria from colonic lumenal content 16S rDNA sequencing data at the phylum level (top 10) between NX and sham rats (Wilcoxon rank-sum test). **f** Comparison of relative abundance of significantly altered bacterial taxa including phylum, class and family levels between sham and NX rats. The Wilcoxon rank sum test was used to determine the significance between groups. $^{*}P<0.05$, $^{**}P<0.01$ versus sham rats. **g** Taxonomic distributions of bacteria from colonic lumenal content 16S rDNA sequencing data at the genus level (top 30) between NX and sham rats (Wilcoxon rank-sum test). **h** The effect of the gut microbiota modifications on predicted functional metabolic pathways obtained from PICRUSt analysis of 16S rRNA sequencing data

comparisons using the Benjamini–Hochberg false discovery rate (FDR) and $P<0.05$ was statistically significant.

Results

General data

Compared to sham rats, the CKD rats showed marked increase in urine output, systolic blood pressure (SBP), diastolic blood pressure (DBP), serum creatinine, urea and proteinuria, while body weight, creatinine clearance (CCr) and hematocrit were evidently decreased (Fig. 1a).

The gut microbiome data

Gut microbiome was determined by Illumina Miseq sequencing using specimen colonic luminal content samples of NX and sham rats. A total of 802 OTUs, with an average of 553 OTUs per sample, were identified from 254,147 quality-filtered sequences in the CKD and sham groups. The α-diversity indexes including Chao1, Shannon and Simpson were used to determine the ecological diversity within microbial community. The Shannon index reflecting both the species richness and evenness was 6.74 ± 0.25 and 6.89 ± 0.19 in sham and CKD rats, respectively (Fig. 1b). The Simpson index reflecting community evenness was 0.023 ± 0.004 and 0.019 ± 0.004 in sham and CKD rats, respectively (Fig. 1b). Significant difference was observed in β-diversity based on the unweighted ($P=0.005$) but not t-weighted ($P=0.270$) UniFrac between the sham and CKD groups (Fig. 1c).

The linear discriminant analysis (LDA) effect size (LEfSe, version 1.0) and Wilcoxon rank sum tests were used to compare the gut microbiota in the sham and CKD rats at different taxonomic levels. CKD altered the structure and composition of the gut microbiota (Table S1). All of the observed sequences could be assigned to 12 phyla. Figure 1d demonstrated the difference in the abundant taxa between samples from sham and CKD rats using phylum- to genus-level data, which indicated the alternation of composition in the sham and CKD rats. Microbiome in both sham and CKD rats were dominated by Firmicutes and Bacteroidetes, which are the typical gut microbiome structures in rats (Fig. 1e). Firmicutes were the most prominent gut bacterial community, accounting for an average of 71.1% and 65.8% sequences in the sham and CKD rats, respectively. Bacteroidetes represented the second dominant gut bacterial community, accounting for an average of 19.9% and 27.5% sequences in the sham and CKD rats, respectively. Other phyla groups including Actinobacteria, Proteobacteria and Verrucomicrobia were detected at low levels (less than 3%) (Fig. 1e). Only the relative abundance of Proteobacteria was significantly increased in CKD rats ($2.28\%\pm0.01\%$) compared to the sham rats ($0.51\%\pm0.01\%$) according to the Wilcoxon rank sum test (Fig. 1f). At the class level, Betaproteobacteria was obviously increased, while Alphaproteobacteria was evidently decreased in CKD rats (Fig. 1f). In addition, enrichments of *Enterobacteriaceae, Sutterellaceae* and *Clostridiaceae_1* as well as the depletion of *Clostridiaceae_2* and *Leuconostocaceae* were observed in CKD rats as well ($P<0.05$ or $P<0.01$) (Fig. 1f).

Alteration of gut taxa in CKD rats

At the genus level, an average of 72.3% sequences per sample could not be assigned to specific genera (Fig. 1g), which is consistent with the previous report [32]. The remaining sequences belonged to 91 genera, among which *Lactobacillus*, *Eubacterium*, *Allobaculum*, *Clostridium XlVa*, *Prevotella*, *Clostridium IV*, *Ruminococcus* and *Romboutsia* were highly abundant in both groups (Fig. 1g). PICRUSt (version 1.1.3) analysis showed that modifications of the gut microbiota affected predicted functional metabolic pathways (Fig. 1h).

LEfSe analysis showed that the CKD rats were mainly characterized by higher abundance of *Allobaculum*, *Escherichia_Shigella*, *Clostridium_sensu_stricto*, *Bacteroides*, *Parasutterella*, *Ruminococcus*, *Blautia* and *Enterorhabdus* (LDA score > 2.0 with $P<0.05$), whereas the sham rats primarily showed higher enrichment of *Pseudomonas*, *Alkaliphilus*, *Leuconostoc*, *Lactococcus* and *Clostridium_IV* (LDA score > 2.0 with $P<0.05$, Fig. 2a, b). Heatmap and orthoPLS-DA showed that these taxa could significantly separate the CKD rats from the sham rats (Figs. 2c; S1). Further, Pearson correlation analysis identified several taxa which was strongly correlated with CKD rats (Fig. 2d). To

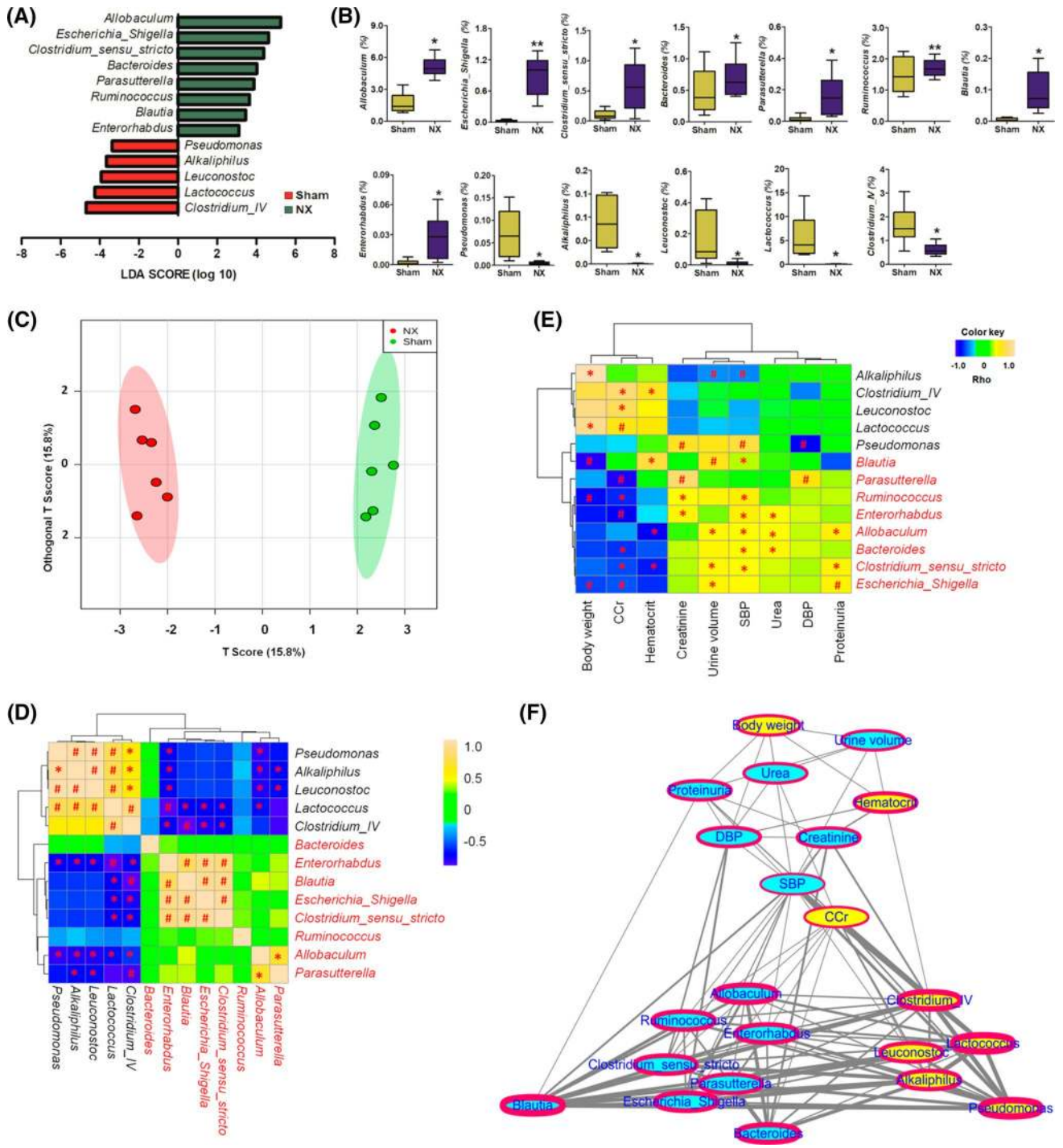

identify correlations between biochemical parameters and changes in the gut microbiome in CKD, we performed a Spearman correlation analysis of altered 13 gut microbiota and biological parameters. We revealed that CCr and SBP were deeply implicated in the alterations of the gut microbiome (Fig. 2e). Spearman correlations between CKD-associated 13 genera as well as nine physiological and biochemical parameters were further observed in a correlation network (Fig. 2f). Additionally, we found SBP and CCr were the hub of the entire network, with two sub-networks produced for physiological parameters and genus (Fig. 2f). The findings showed that significant positive correlations between increased proteinuria with *Blautia* and decreased hematocrit with *Clostridium_IV* were independent of CCr. Taken together, these results indicated that renal dysfunction could influence the structure and composition of gut microbiota. In turn, gut microbiota dysbiosis played paramount roles in the deterioration of impaired renal function.

◂**Fig. 2** Significantly altered bacterial taxa in CKD rats. **a** LDA score of the significantly discriminant genera between the two groups (LDA score > 2.0, Wilcoxon rank-sum tests, $P < 0.05$). **b** Boxplots showing differences in the relative abundance of 13 significantly discriminant taxa driving gut microbiome differences between NX and sham rats. $^{*}P < 0.05$, $^{**}P < 0.01$ versus sham rats ($n = 6$). **c** orthoPLS-DA plots with the scores of the first two principal components based on 13 taxa from the NX and sham rats. **d** Correlations of 13 significantly discriminant taxa in NX and sham rats using Spearman correlation analysis. Asterisks denoted statistical significance between bacterial taxa, $^{*}P < 0.05$, $^{\#}P < 0.01$. **e** Spearman's rank correlation between 13 most differential genera selected from the LEfSe and clinical biochemical parameters. The results were presented as a heatmap using Ward clustering analysis. Heatmap showed that microbial taxa was intimately associated with metabolites, which was positively or negatively related to clinical chemistry. Rho in the color key represented Spearman rank correlation coefficient. $^{*}P < 0.05$, $^{\#}P < 0.01$ denoted statistical significance between bacterial taxa and biochemical parameters. **f** The construction of correlation network by using the perfuse force directed layout in the Cytoscape software. The nodes of the network represented the genera and clinical indices, where the edges corresponded to a significant ($P < 0.05$) and positive (blue) or negative (yellow) correlation between the nodes. The border width of the nodes and edges (connections) represented relative abundance of clinical parameters and bacterial taxa

Potential functional impact of CKD-induced changes in the gut microbiome

To predict the possible impact of the altered gut microbiome in CKD rats, OTUs were assigned to the closest reference genome in the database from the PICRUSt analysis. PICRUSt analysis showed that 471 KEGG orthology (KO) were associated with 219 altered metabolic pathways, such as lipid biosynthesis and metabolism (sphingolipids, fatty acids, steroids, bile acids), amino acid biosynthesis and metabolism (valine, leucine, isoleucine biosynthesis, phenylalanine, tyrosine, tryptophan and histidine), aminobenzoate degradation, phenylpropanoid biosynthesis and MAPK signaling pathway (Table S3), which are associated with 37 enzymes (Table S4). The metabolic pathways and associated enzymes were involved in alternation of 33 metabolic pathways (Fig. 1h). Gut microbiome was involved in the production of the uremic toxins including p-cresyl sulfate (PCS) and indoxyl sulfate (IS) which contributed much to systemic inflammation, impairment of intestinal barrier structure/function, and the progression of CKD [33]. Gut microbes can convert phosphatidylcholine and L-carnitine into trimethylamine which was metabolized by hepatic flavin monooxygenase to trimethylamine N-oxide (TMAO) and finally excreted by the kidney [34]. TMAO was closely involved in renal fibrosis as well as CKD progression and its complications, such as atherosclerosis and CVD [14]. The KO for enzymes were responsible for the production of uremic toxins, such as the tryptophanase, tyrosine phenol-lyase gene, and the production of TAMO was searched within the closest reference genome of each OTU (Table S2). A total of nine OTUs were found to contain the genes encoding tryptophanase (K01667) and/or tyrosine phenol-lyase (K01668) in their closest reference genome (Table S2), of which three OTUs were assigned to the Proteobacteria phylum (OTUs 54, 189, and 778) and four OTUs were assigned to the Bacteroidetes (OTU 166, 233, 535, and 888) phylum, while one OTU was assigned to the Elusimicrobia (OTU 769) and Verrucomicrobia (OTU 173) phylums. Genes related to the production of trimethylamine (TMA), including K07811 (trimethylamine oxidoreductase 1), K07821 (trimethylamine oxidoreductase 2, c-type cytochrome subtribe activity regulation transducer), and K03532 (trimethylamine oxidoreductase 1, c-type cytochrome subtribe activity regulation transducer) were found in closest genome of the following five OTUs: *Escherichia fergusonii*, *Aggregatibacter aphrophilus* NJ8700, *Psychrobacter* sp. PRwf-1, *Desulfovibrio fairfieldensis* and *Helicobacter typhlonius*, all of which belonged to the Proteobacteria phylum. These species were the candidate bacteria producing uremic toxins in the rat's intestinal tract, among which *Escherichia fergusonii* and *Bacteroides thetaiotaomicron* were significantly increased in the CKD rats compared to control rats.

Alteration of serum metabolome in CKD rats

UPLC–HDMS was used to identify the metabolite profiles in both positive and negative ion modes. We observed higher noise and matrix effect resulting in a high baseline in the negative ion mode. Therefore, positive ion mode was applied for final analysis and 7389 variables were revealed. Score plots of OPLS-DA showed that CKD rats could be separated from sham rats (Fig. 3a). 1772 variables were selected based on S-Plot (Fig. 3b), $P < 0.05$ (Table S5), adjusted FDR (Table S5) and coefficient analyses (Fig. 3c). 291 metabolites were identified based on criteria established in our previously reported methods [35–37] (Table S5). They could differentiate CKD rats from sham rats (Fig. 3d–f) and as shown in Fig. 3g, these metabolites were mainly involved in fatty acid metabolism (branched chain fatty acid oxidation, linoleic acid, fatty acyl-CoA biosynthesis), amino acid metabolism (tryptophan, tyrosine, phenylalanine, histidine, lysine, proline, etc.), polyamine metabolism (spermidine and spermine biosynthesis) and purine metabolism. Of note, the majority of metabolic pathways were associated with the gut microbial metabolism, indicating the dysbiosis of gut microbiota in CKD rats. Moreover, pathway-associated metabolic networks indicated that dysregulations of the metabolic pathways were also related to the metabolism of methylhistidine, phenylalanine, tyrosine, glycine, serine, tryptophan and butyrate as well as the biosynthesis of spermidine, spermine, phospholipid and fatty acid (Figs. S2A, S2B, S3 and Table S6). Taken together, CKD was closely associated with altered amino acid, polyamine and lipid metabolisms.

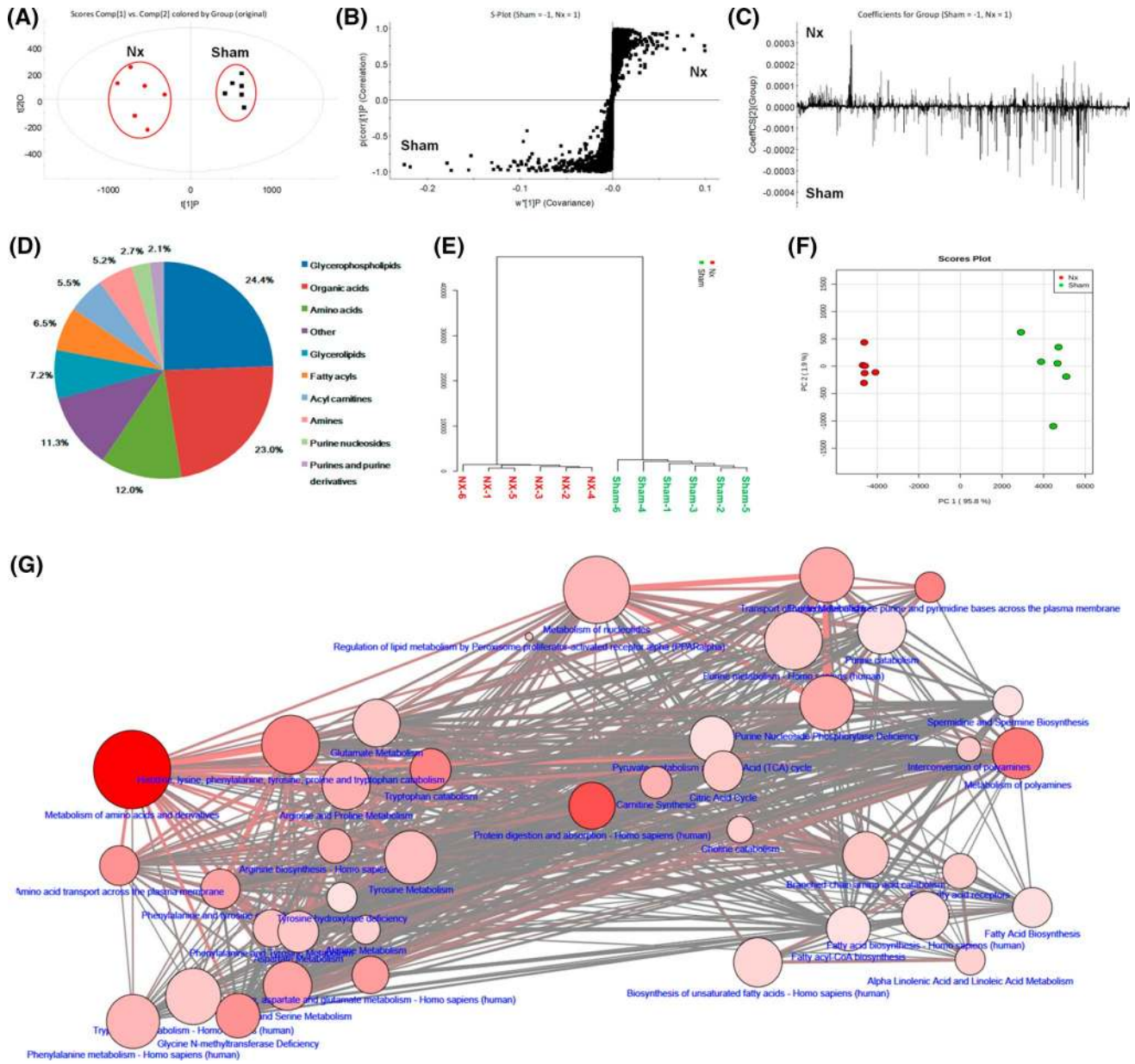

Fig. 3 Metabolic profile as well as multivariate analysis and metabolic pathway of metabolites in NX rats. **a** OPLS-DA plots with the scores of the first two principal components. **b** S-plots of OPLS-DA model from the NX and sham rats. **c** Loading plots of OPLS-DA model from the NX and sham rats. **d** Dendrogram analysis based on 291 metabolites. **e** Heatmap analysis of 291 metabolites. **f** PCA plots with the scores of the first two principal components based on 291 metabolites. **g** Metabolite pathway analysis of 291 metabolites by MetScape software running on cytoscape based on KEGG, Reactome and SMPDB database. The border width of the nodes and edges (connections) represented relative abundance of clinical parameters and bacterial taxa

Association of the CKD-induced gut microbial dysbiosis with dysregulation metabolites

To further investigate the potential role of the altered gut microbiota in the pathogenesis of altered metabolites, we performed a Spearman correlation analysis. As shown in Fig. 4a, 36 metabolites were significantly associated with 13 altered microbial genera. Decreased tyrosine and tryptophan showed a positive correlation with *Clostridium_IV* and a negative correlation with *Allobaculum*, *Clostridium_sensu_stricto*, *Escherichia_Shigella*, *Enterorhabdus* and *Blautia*. Most of metabolites such as TMAO, glycine, cinnamoylglycine, phenylacetylglycine, phenylpropionylglycine, spermine, spermidine, acrolein, putrescine and N1-acetylspermidine were obviously increased in CKD rats and showed a positive correlation with *Clostridium_sensu_stricto*,

Escherichia_Shigella, *Enterorhabdus*, *Parasutterella* and *Blautia* that harbored genes encoding enzymes involved in glycine-conjugated metabolites and polyamine metabolism.

Spearman correlation analysis was performed using SBP and 36 metabolites. Figure 4b presented the relative intensities determined by metabolomic method and *P* values (< 0.05) were calculated by Spearman correlation analysis based on the values of SBP and relative intensities of 16 metabolites. The Spearman correlation analysis revealed that SBP was associated with 16 metabolites. Interestingly, ten compounds, such as cinnamoylglycine, 2-phenylacetic acid, phenylacetylglycine, phenylpropionylglycine and hippuric acid, were glycine-conjugated microbial metabolites (Fig. 4c). For example, hippuric acid was produced by the conjugation of benzoic acid with glycine, a reaction that occurred in the liver, kidney and intestine. The glycine could directly conjugate to phenylpropionic acid, a known metabolic byproduct of anaerobic bacteria. However, phenylpropionic acid was normally converted to benzoic acid by β-oxidizing medium-chain acyl-CoA dehydrogenase in humans. These findings demonstrated that glycine bioactivity was partly associated with CKD-induced hypertension. Increased glycine-conjugated metabolites including cinnamoylglycine, phenylpropionylglycine, 2-phenylacetic acid and hippuric acid showed strong positive correlations with *Escherichia_Shigella*, *Enterorhabdus*, *Parasutterella* and *Bacteroides*, as well as strong negative correlation with *Clostridium_IV*, which possessed genes encoding glycine dehydrogenase (K00281), glycine oxidase (K03153), glycine reductase (K10670) and 3-phenylpropionate/cinnamic acid dioxygenase subunit α (K05708) as well as their corresponding enzymes (EC:1.4.4.2), (EC:1.4.3.19), (EC:1.21.4.2) and (EC:1.14.12.19) that converted spermine or spermidine to other polyamines (Fig. 4b).

Increased spermine, spermidine, acrolein, N1-acetylspermidine and N1,N12-diacetylspermine in CKD rats were mainly implicated in the enrichments of *Clostridium_sensu_stricto*, *Escherichia_Shigella*, *Enterorhabdus* and *Parasutterella*, which possessed genes encoding spermine synthase (K00802), spermidine synthase (K00797), spermidine dehydrogenase (K00316), homospermidine synthase (K00808) and putative spermidine/putrescine transport system permease protein (K02053) as well as their corresponding enzymes (EC:2.5.1.22), (EC:2.5.1.16), (EC:1.5.99.6) and (EC:2.5.1.44) that converted spermine or spermidine to other polyamines (Fig. 5b). However, increased putrescine was only associated with *Bacteroides*, which possessed genes encoding putrescine aminotransferase (K09251, K12256), spermidine/putrescine transport system permease protein (K11070, K11071) and putrescine carbamoyltransferase (K13252) as well as their corresponding enzymes (EC:2.6.1.82), (EC:2.6.1.-) and (EC:2.1.3.6) that converted spermidine to putrescine (Fig. 5b).

Metabolic network modeling and microbiome–metabolite associations in gut microbiota–metabolite–phenotype axis

To assess the potential role of the altered metabolites with renal function, we performed a Spearman correlation and linear regression analyses of CCr and metabolites using gut microbiota-associated 36 metabolites. 15 metabolites showed a significant correlation with CCr and had linear regression coefficient of more than 0.800 (Fig. 5a). Of note, these metabolites belonged to polyamine metabolism (spermine, spermidine, acrolein, putrescine, 3-aminopropanal, *N*1-acetylspermidine and *N*1,*N*12-diacetylspermine). Polyamines have been identified as uremic toxins, which accelerate progression of renal fibrosis [38]. Figure 5b presented the polyamine metabolism pathway in CKD rats.

The influence of gut microbiota on the host's metabolic activity has been studied widely, which contributes much on both local and systemic metabolism. To further explore the association among clinical indices, bacterial genus and metabolites, a network analysis based on nine clinical indices, 13 genus-level bacterial taxa, seven metabolites in glycine metabolic pathway and six metabolites in polyamine metabolism was used to highlight the associations of the gut microbiome with clinical indices and serum metabolites in renal fibrosis by Cytoscape software (version 3.6.1). As shown in Fig. 5c, CCr was directly linked to dysbiosis of gut microbiota, clinical indices and metabolites, which indicated that the renal function decline was associated with microbial composition, glycine metabolism and polyamine metabolism that contributed to renal fibrosis. Gut microbiota was deeply implicated in glycine metabolism and polyamine metabolism. Interestingly, hypertension exhibited a higher positive correlation with the dysregulation of glycine metabolism and microbiome; however, CCr had a higher negative correlation with upregulated polyamine metabolism and microbiome in NX rats, underscoring the connection between strong variations in microbial abundance and metabolic regulation in NX rats.

Effects of PAA and *Poria cocos* (PC) administration on gut microbiome, serum metabolites and renal fibrosis in CKD rats

To demonstrate whether gut microbiome could affect renal fibrosis, CKD rats were treated with PC, a well-known natural fungus with marked antioxidative, antiinflammatory, antibacterial, diuretic and antifibrotic effects on CKD [39–45]. PAA is a major tetracyclic triterpenoid derivative of PC [46–48]. As shown in Fig. 6a, b, treatment with both PAA and PC improved glycine and polyamine metabolisms in CKD rats. Interestingly, PAA treatment showed a stronger effect on glycine metabolism than that of PC., while

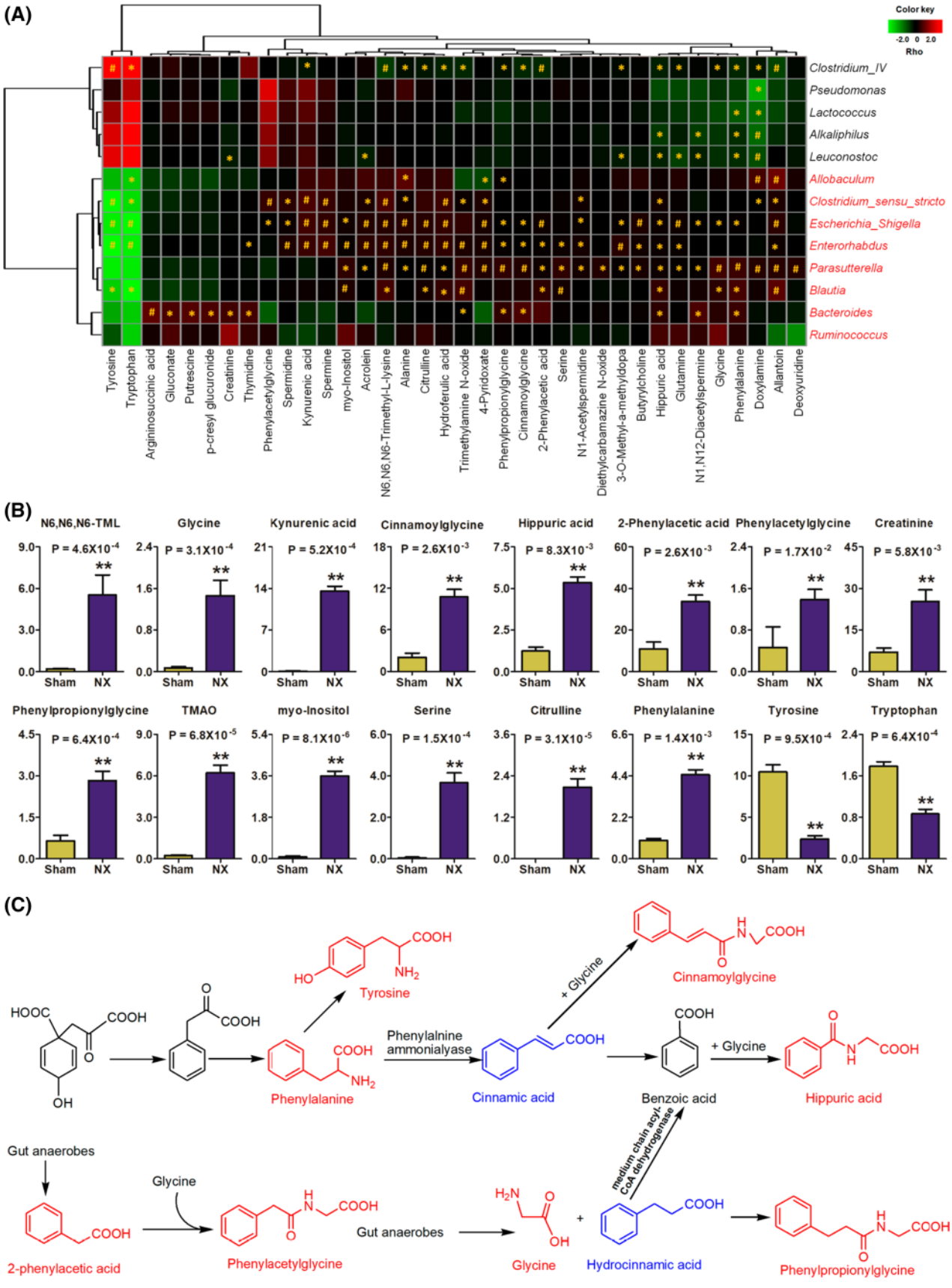
(A)
Color key
-2.0 0 2.0
Rho
Clostridium_IV
Pseudomonas
Lactococcus
Alkaliphilus
Leuconostoc
Allobaculum
Clostridium_sensu_stricto
Escherichia_Shigella
Enterorhabdus
Parasutterella
Blautia
Bacteroides
Ruminococcus
Tyrosine
Tryptophan
Argininosuccinic acid
Gluconate
Putrescine
p-cresyl glucuronide
Creatinine
Thymidine
Phenylacetylglycine
Spermidine
Kynurenic acid
Spermine
myo-Inositol
Acrolein
N6,N6,N6-Trimethyl-L-lysine
Alanine
Citrulline
Hydroferulic acid
Trimethylamine N-oxide
4-Pyridoxate
Phenylpropionylglycine
Cinnamoylglycine
2-Phenylacetic acid
Serine
N1-Acetylspermidine
Diethylcarbamazine N-oxide
3-O-Methyl-a-methyldopa
Butyrylcholine
Hippuric acid
Glutamine
N1,N12-Diacetylspermine
Glycine
Phenylalanine
Doxylamine
Allantoin
Deoxyuridine
(B)
N6,N6,N6-TML
P = 4.6X10-4
Glycine
P = 3.1X10-4
Kynurenic acid
P = 5.2X10-4
Cinnamoylglycine
P = 2.6X10-3
Hippuric acid
P = 8.3X10-3
2-Phenylacetic acid
P = 2.6X10-3
Phenylacetylglycine
P = 1.7X10-2
Creatinine
P = 5.8X10-3
Phenylpropionylglycine
P = 6.4X10-4
TMAO
P = 6.8X10-5
myo-Inositol
P = 8.1X10-6
Serine
P = 1.5X10-4
Citrulline
P = 3.1X10-5
Phenylalanine
P = 1.4X10-3
Tyrosine
P = 9.5X10-4
Tryptophan
P = 6.4X10-4
Sham
NX
(C)
Tyrosine
Phenylalanine
Phenylalnine ammonialyase
Cinnamic acid
+ Glycine
Cinnamoylglycine
Benzoic acid
+ Glycine
Hippuric acid
Gut anaerobes
2-phenylacetic acid
Glycine
Phenylacetylglycine
Gut anaerobes
Glycine
medium chain acyl-CoA dehydrogenase
Hydrocinnamic acid
Phenylpropionylglycine

◂**Fig. 4** Correlation analysis of the gut microbiome and serum metabolites as well as relationship between hypertension and serum metabolites. **a** Spearman's rank correlation between 13 most differential genera and 36 differential metabolites (metabolite that correlated with at least one genus with $P < 0.05$ was shown). The results were presented as a heatmap using Ward clustering analysis. The scale ranged from +2.0 (red) to −2.0 (green). Heatmap showed that microbial taxa was correlated with metabolites, which linked positively or negatively to renal fibrosis in NX rats. Rho in the color key represented Spearman rank correlation coefficient. $^{*}P < 0.05$, $^{\#}P < 0.01$ denoted statistical significance between bacterial taxa and metabolites. **b** Relative intensity of individual metabolites in NX and sham rats. 16 metabolites were selected by correlation analysis between metabolites and SBP ($P < 0.05$). *P* value was calculated by Spearman rank correlation. Vertical axis was the relative intensity of individual metabolites. Asterisks denoted statistical significance between NX and sham rats, $^{**}P < 0.01$ versus the relative intensity of the sham rats. **c** Analysis of the metabolites in glycine pathway. The relative intensities in the serum metabolites were shown in boxes. Metabolites highlighted by red indicated the identified metabolites and their relative intensities were presented in **b** in current study

PC treatment was relatively more prominent on polyamine metabolism compared to PAA. In addition, emerging evidence suggested that altered gut microbiota was, in part, responsible for the pathogenesis of hypertension, accumulation of uremic toxin and the decline in kidney function [8, 9, 49]. It was speculated that PAA improved renal function and attenuated interstitial fibrosis partly by lowering blood pressure. However, PC improved renal function and reduced fibrosis partly by lessening the generation of polyamine-derived uremic toxins. Present study showed that treatment with both PAA and PC could attenuate CKD and its consequences (Fig. 6c). Notably, PAA treatment showed a stronger effect on improving renal function than PC, which indicated the contribution of hypertension on CKD progression. Moreover, both PAA and PC treatment can upregulate the protein expression of ZO1, occludin and claudin-1 (Fig. 6d, e).

The breakdown of the gut epithelial barrier triggered local and systemic inflammation and influx of leukocytes as well as accelerated the translocation of uremic toxins into the systemic circulation in CKD patients and animals [8]. NX rats exhibited a significant upregulation in nuclear translocation of p65, pointing to the activation of NF-κB signaling (Fig. 7a). Activation of IκBα/NF-κB was accompanied by marked upregulation of inflammatory proteins including MCP-1 and COX-2, as well as the downregulation of antioxidative system including Nrf2 and its downstream gene products, such as HO-1, catalase and NQO1 (Fig. 7a–d). Both PAA and PC treatment inhibited the upregulation of IκB/NF-κB pathway and prevented the downregulation of cytoprotective Keap1/Nrf2 pathway. Interestingly, PAA showed a stronger effect on these pathways than that of PC (Fig. 7a–d).

Oxidative stress and inflammation played paramount roles in the pathogenesis and progression of CKD [29, 50, 51]. Compared to sham rats, the CKD rats showed interstitial inflammatory cell infiltration and tubular atrophy/dilatation (Fig. 7e). Histological analysis indicated that both PAA and PC treatment significantly attenuated renal injury (Fig. 7f). Immunohistochemical staining showed that treatment with both PAA and PC inhibited the upregulation of profibrotic factors including α-SMA, vimentin and collagen I (Fig. 7e). Interestingly, PAA showed a stronger antifibrotic effect than that of PC. Taken together, these results suggest that PAA and PC treatment could ameliorate inflammation and oxidative stress as well as retard renal fibrosis in the CKD rats by attenuating microbial dysbiosis, preventing disruption of intestinal epithelial barrier, and mitigating dysregulation of serum metabolites.

Discussion

The present study demonstrated profound changes of the gut microbiome marked by altered composition and reduced diversity of the bacterial population in CKD rats, which was highly consistent with the earlier studies [9]. In confirmation of the previous studies, microbial dysbiosis in CKD rats was accompanied by marked alteration of plasma metabolome [52]. The microbial-derived metabolites were closely linked to the inflammation and oxidative stress in CKD rats. A growing body of evidence demonstrated that dietary supplementation of amylose, a plant-derived indigestible complex carbohydrate, ameliorated oxidative stress as well as inflammation and retarded the progression of chronic kidney disease in CKD rats [53]. Additionally, amylose improved microbial dysbiosis and metabolomic profiles [52] in rats with adenine-induced chronic interstitial nephropathy as well. Present study reveals that dietary supplementation of the prebiotics, PC and PAA could ameliorate microbial dysbiosis, lower the related toxic metabolites, mitigate interstitial fibrosis and retard the decline of renal function in rats with CKD induced by 5/6 nephrectomy. Significant changes in the abundance of 13 bacterial species including *Blautia*, *Escherichia_Shigella*, *Bacteroides*, *Allobaculum* and *Clostridium_IV*, and 291 metabolites were observed in CKD rats, highlighting the critical impact of CKD on the gut microbiome and its role in dysregulated metabolites.

Dysbiosis of the gut microbiota has been described previously in CKD rats and humans [9, 32]. Using phylogenic microarray technique, in a previous study we compared the composition of the bacterial community in fecal samples of rats with CKD induced by 5/6 nephrectomy with that of sham-operated control rats. The study revealed reduced richness and distinct changes in composition of bacterial community structure in CKD rats [9]. In a subsequent study,

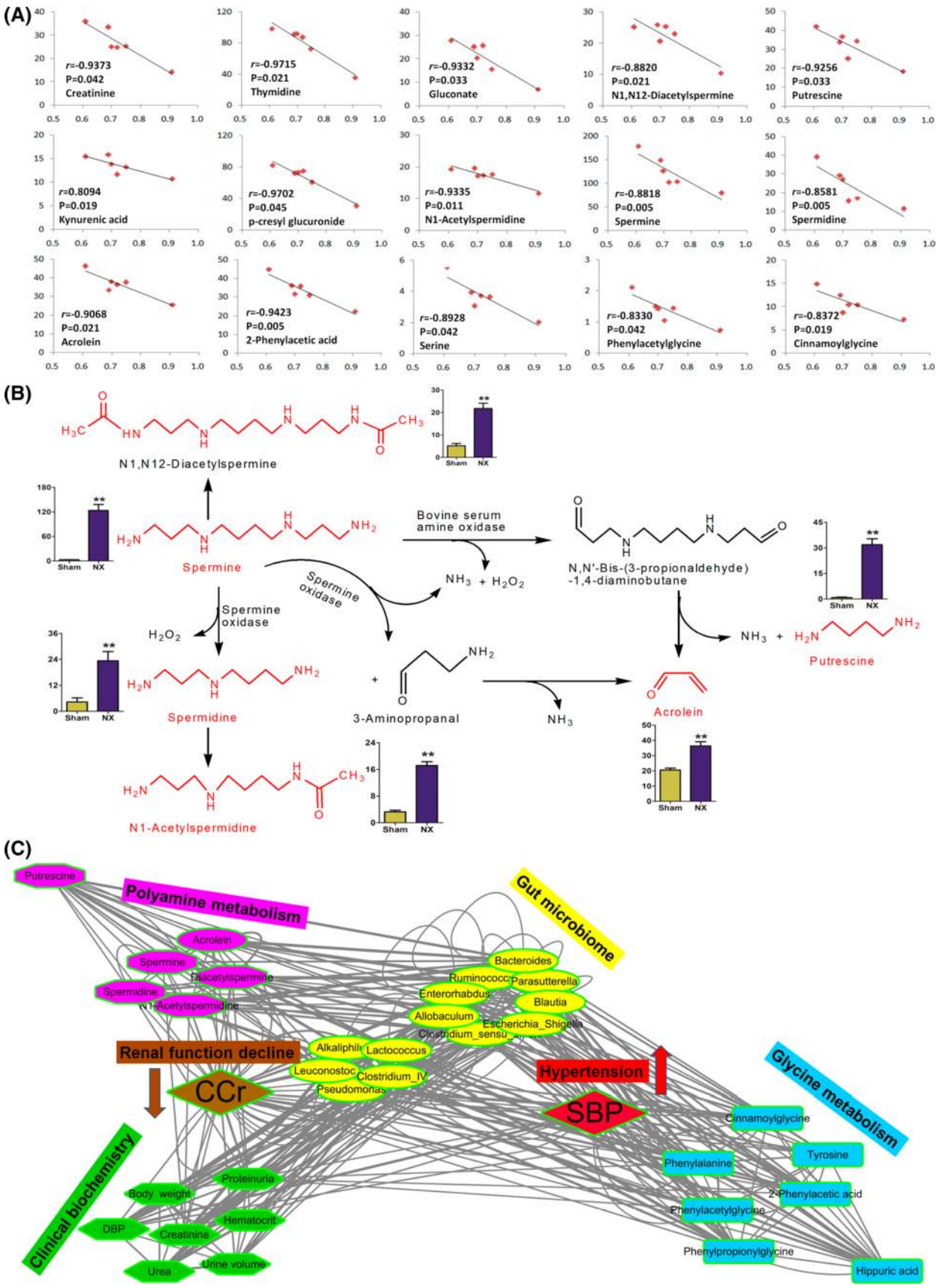
(A)
r=-0.9373
P=0.042
Creatinine
r=-0.9715
P=0.021
Thymidine
r=-0.9332
P=0.033
Gluconate
r=-0.8820
P=0.021
N1,N12-Diacetylspermine
r=-0.9256
P=0.033
Putrescine
r=0.8094
P=0.019
Kynurenic acid
r=-0.9702
P=0.045
p-cresyl glucuronide
r=-0.9335
P=0.011
N1-Acetylspermidine
r=-0.8818
P=0.005
Spermine
r=-0.8581
P=0.005
Spermidine
r=-0.9068
P=0.021
Acrolein
r=-0.9423
P=0.005
2-Phenylacetic acid
r=-0.8928
P=0.042
Serine
r=-0.8330
P=0.042
Phenylacetylglycine
r=-0.8372
P=0.019
Cinnamoylglycine
(B)
N1,N12-Diacetylspermine
Spermine
Bovine serum amine oxidase
N,N'-Bis-(3-propionaldehyde) -1,4-diaminobutane
Spermine oxidase
NH3 + H2O2
Spermine oxidase
H2O2
Spermidine
3-Aminopropanal
NH3
Acrolein
NH3 + Putrescine
N1-Acetylspermidine
Sham
NX
(C)
Putrescine
Polyamine metabolism
Gut microbiome
Acrolein
Spermine
Diacetylspermine
Spermidine
N1-Acetylspermidine
Bacteroides
Ruminococc
Parasutterella
Enterorhabdus
Blautia
Allobaculum
Escherichia_Shigella
Clostridium_sensu
Alkaliphil
Lactococcus
Leuconostoc
Clostridium_IV
Pseudomonas
Renal function decline
CCr
Hypertension
SBP
Glycine metabolism
Cinnamoylglycine
Tyrosine
Phenylalanine
2-Phenylacetic acid
Phenylacetylglycine
Phenylpropionylglycine
Hippuric acid
Clinical biochemistry
Proteinuria
Body weight
DBP
Creatinine
Hematocrit
Urea
Urine volume

◂**Fig. 5** Associations of the gut microbiome with clinical indices and serum metabolites in renal fibrosis. **a** The associations between CCr and taxa-associated significant metabolites in NX rats. *r* indicated the linear coefficients. Metabolites were selected based on $R > 0.800$. The values of *P* were calculated by Spearman rank correlation between CCr and metabolites. **b** Analysis of the metabolites of the spermine pathway. The relative intensities in the serum metabolites were shown in boxes. Metabolites highlighted by red indicated the identified metabolites in current study. **c** Correlation network among 13 genus-level bacterial taxa, nine clinical indices and seven metabolites in glycine metabolic pathway and six metabolites in polyamine metabolism by Cytoscape software. The nodes of the network represented the genera (yellow circle), clinical indices (green hexagon) and glycine metabolites (blue rectangle) as well as polyamine metabolites (pink octagon), where the edges corresponded to a significant ($P < 0.05$) and positive (Spearman rho < -0.3) or negative (Spearman rho > 0.3) correlation between the nodes

Kikuchi et al. [32] found reduced diversity and altered composition of the gut microbial community in the fecal samples of NX rats compared to those of sham-operated control rats. In confirmation of the above studies, Firmicutes, Bacteroidetes, Proteobacteria and Actinobacteria were the most dominant bacterial phylum in the colon content from our rats. As expected, the CKD rats showed significant alternation of the gut microbiome. In particular, at the genus level, we found the enrichment of *Enterorhabdus*, *Blautia*, *Ruminococcus*, *Parasutterella*, *Bacteroides*, *Clostridium_sensu_stricto*, *Escherichia_Shigella* and *Allobaculum*, and the depletion of *Clostridium_IV*, *Lactococcus*, *Leuconostoc*, *Alkaliphilus* and *Pseudomonas* in our CKD rats. These findings confirmed the concurrence of gut microbial dysbiosis in CKD. One of the striking changes of the microbiome in CKD rats employed in the present study and in CKD rats and ESRD patients in previous studies [32, 54] is enrichment of *Escherichia_Shigella* which consists of one of the species assigned to *Escherichia fergusonii*. *E. fergusonii* is an enterotoxin-producing bacterium responsible for a wide variety of intestinal and extra-intestinal infections in animals and humans [55, 56]. Enrichment of the *E. fergusonii,* an aerobic bacterium in our CKD rats, is consistent with the

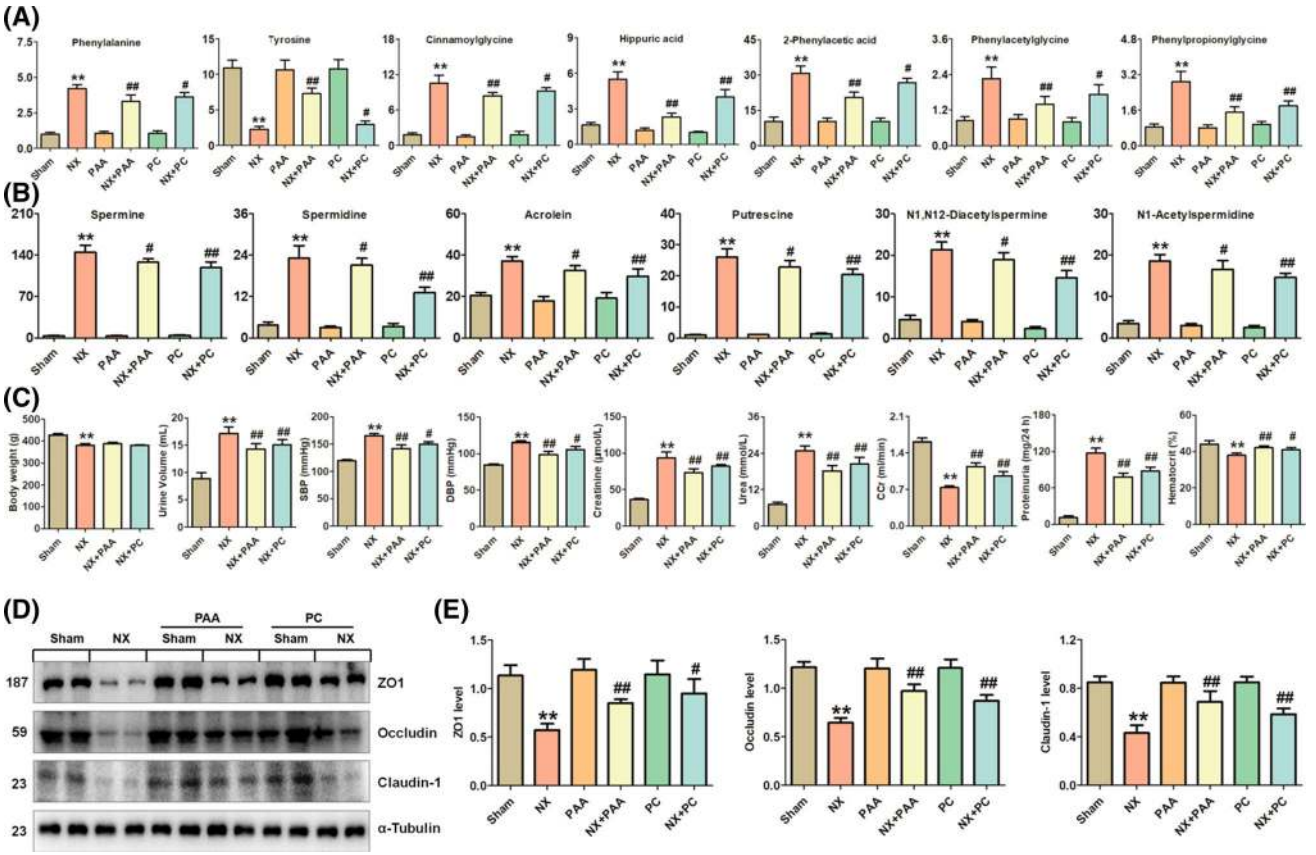

Fig. 6 Effects of PAA and PC on serum metabolites, clinical indices and intestinal barrier in NX rats. **a** Relative intensity of individual glycine metabolites in the serum of the different rats. Vertical axis was the relative intensity of individual metabolites. **b** Relative intensity of individual polyamine metabolites in the serum of the different rats. Vertical axis was the relative intensity of individual metabolites. **c** Clinical indices of the different rats. **d** The expression levels of the tight junction protein expressions including ZO1, occludin and claudin-1 in the colon of the different rats. Tissue lysates were immunoblotted with specific antibodies against ZO1, occludin and claudin-1. **e** Graphic representations of ZO1, occludin and claudin-1 expression in different groups as indicated. $^{*}P < 0.05$; $^{**}P < 0.01$ versus sham rats ($n = 6$); $^{\#}P < 0.05$, $^{\#\#}P < 0.01$ versus NX rats ($n = 6$)

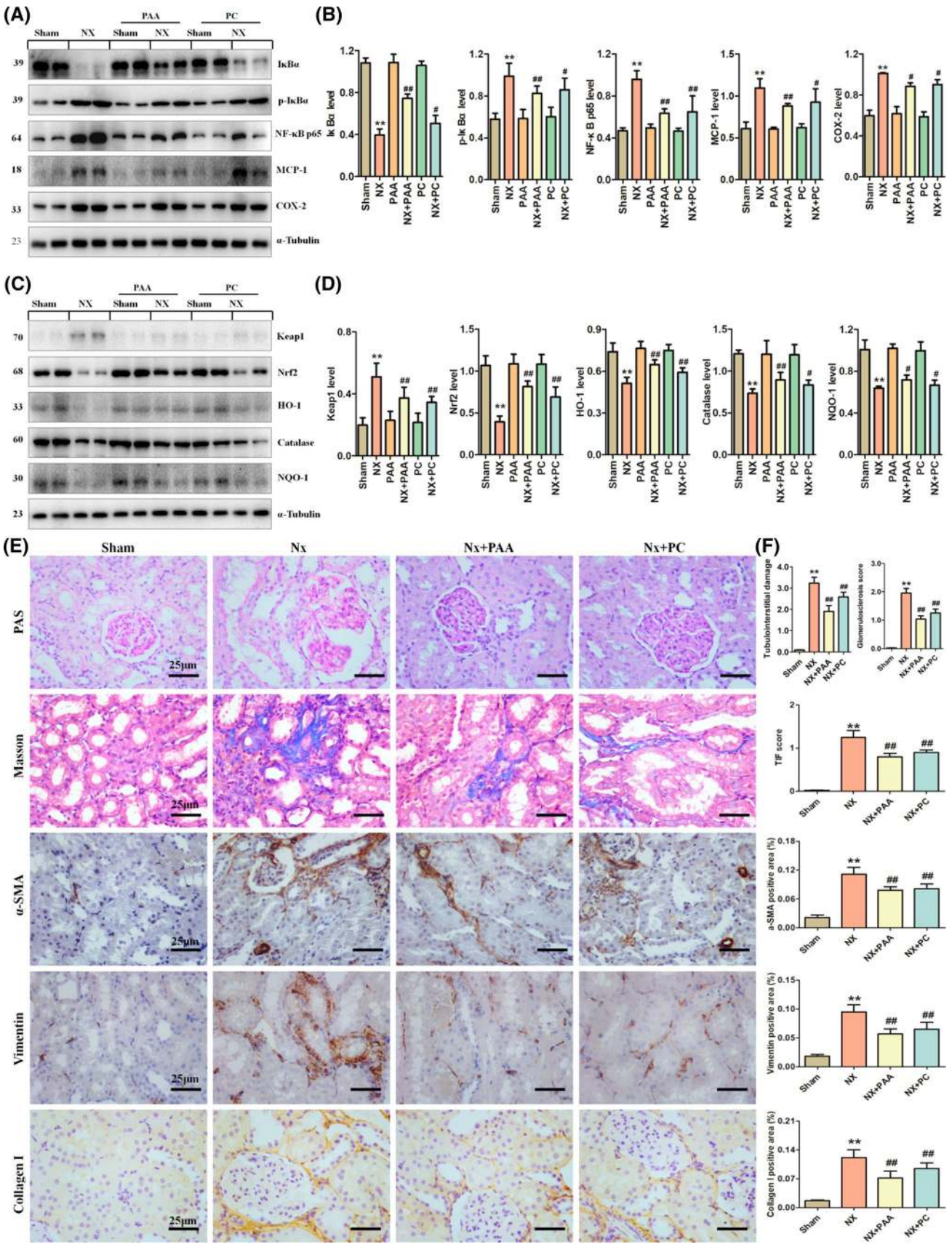
(A)
Sham
NX
PAA
PC
IκBα
p-IκBα
NF-κB p65
MCP-1
COX-2
α-Tubulin
(B)
Ik Bα level
p-Ik Bα level
NF-κ B p65 level
MCP-1 level
COX-2 level
(C)
Keap1
Nrf2
HO-1
Catalase
NQO-1
(D)
Keap1 level
Nrf2 level
HO-1 level
Catalase level
NQO-1 level
(E)
Sham
Nx
Nx+PAA
Nx+PC
PAS
Masson
α-SMA
Vimentin
Collagen I
25μm
(F)
Tubulointerstitial damage
Glomerulosclerosis score
TIF score
α-SMA positive area (%)
Vimentin positive area (%)
Collagen I positive area (%)

◂**Fig. 7** Effects of PAA and PC on inflammation and TIF in NX rats. **a** Western blot depicting IκBα, p-IκBα and nuclear content of p65 active subunit of NF-κB and expression of COX-2 and MCP-1 in kidney tissues of different rats. Tissue lysates were immunoblotted with specific antibodies against IκBα, p-IκBα, NF-κB, COX-2 and MCP-1. **b** Graphic representations of IκBα, p-IκBα, NF-κB, COX-2 and MCP-1 expression in different groups. **c** Western blot depicting nuclear translocation of Nrf2 and protein abundances of its repressor, Keap1, and its downstream gene products, such as catalase, HO-1 and NQO-1 expression in kidney tissues of different rats. Tissue lysates were immunoblotted with specific antibodies against Keap1, Nrf2, catalase, HO-1 and NQO-1. **d** Graphic representations of Keap1, Nrf2, catalase, HO-1 and NQO-1 expression in different groups. **e** Images of PAS staining, Masson's Trichrome staining and immunohistochemical staining of α-SMA, vimintin and collagen I expression in different rats. **f** Graphic representations of PAS staining including tubulointerstitial damage, glomerulosclerosis score, Masson's Trichrome staining and immunohistochemical staining in different groups. $^{*}P<0.05$; $^{**}P<0.01$ versus sham rats ($n=6$); $^{\#}P<0.05$, $^{\#\#}P<0.01$ versus NX rats ($n=6$)

previously demonstrated expansion of aerobic bacteria in the hemodialysis patients [57]. In addition, *E. fergusonii*'s genome contains genes encoding enzymes capable of producing the gut-derived uremic toxins IS, p-CS and TMAO, pointing to the potential effect of *E. fergusonii* on uremic toxin production in the rats' intestine.

The *Blautia* population was markedly elevated in our CKD rats, which provided additional evidence to the earlier study reported by Zeng et al. [58]. In addition, the rise in *Blautia* has been shown to be associated with early decline in renal function (eGFR decline) in a large cohort of patients with minimal renal dysfunction [59]. Vancomycin administration in ESRD patients has been shown to significantly reduce *Blautia*, and lower serum IS and p-CS levels at day 7 followed by their rebound to or above baseline values at day 28 [60]. IS and PCS are the byproducts of tryptophan and tyrosine metabolism by the gut bacteria and their rise within 28 days following vancomycin therapy in ESRD patients points the resilience of the taxa generating these toxins [60].

Increased abundance of *Ruminococcus* and *Allobaculum* genera observed in our CKD rats is consistent with the previously reported findings in mice with adenine-induced CKD and rats with 5/6 nephrectomy-induced CKD [32, 58, 61]. Moreover, consumption of high-fiber diets has been shown to obviously reduce the abundance of *Ruminococcus* and *Allobaculum* in rats with adenine-induced CKD [52]. Moreover, other study showed that *Ruminococcus* was positively correlated with eGFR decline in CKD patients [62]. The increased abundance of the fragments of *Bacteroides* genera has been reported in the blood samples of ESRD patients [63] and patients with kidney stone [64]. Interestingly, the alternation of *Blautia*, *Bacteroides*, *Escherichia_Shigella* and *Allobaculum* has been reported in rats with spontaneous hypertension [65], coinciding with our findings in CKD rats which had hypertension. Our CKD rats had increased abundance of *Parasutterella.*

In our CKD rats, we found depletion of *Clostridium IV* bacteria which produced short-chain fatty acid (SCFA), especially butyrate that had antiinflammatory and protective effects on the colonic epithelium [66]. Most of the *Clostridium IV* OTUs could not be identified as specific species, indicating that unknown *Clostridium* spp. was involved in the maintenance of gut bacterial homeostasis. Colonic colonization of Clostridium spp. was related to accumulation of Treg lymphocytes which inhibited the development of inflammatory lesions [67]. Two *Clostridium IV* species including *Clostridium leptum* and *Eubacterium siraeum* were significantly decreased in our CKD rats. *C. leptum* can induce stimulation of Treg cells and inhibit the inflammatory response [68]. The observed depletion of the antiinflammatory bacteria may contribute to the inflammatory state in CKD rats. Pseudomonas genus was evidently decreased in our CKD rats, which was consistent with previous studies in ESRD patients [69]. The enrichment of Lactococcus and Leuconostoc were observed in our study as well. Tain et al. [70] reported the association of increased Lactococcus and decreased Leuconostoc with the development of hypertension by maternal and post-weaning high-fructose diets in adult offspring.

Dysbiosis of the gut microbiota in our CKD rats was accompanied by the alteration of serum metabolome. Correlation analysis demonstrated that increased spermine, spermidine, acrolein, *N*1-acetylspermidine and *N*1,*N*12-diacetylspermine were mainly associated with the enrichment of microbial genera which possess the genes encoding spermine synthase, spermidine synthase, spermidine dehydrogenase and homospermidine synthase, putative spermidine/putrescine transport system permease protein and their corresponding enzymes (EC:2.5.1.22), (EC:2.5.1.16), (EC:1.5.99.6) and (EC:2.5.1.44) that convert spermine or spermidine to other polyamines. However, increased putrescine was only associated with *Bacteroides* which possesses genes encoding putrescine aminotransferase and putrescine carbamoyl transferase as well as their corresponding enzymes [(EC:2.6.1.82), (EC:2.6.1.-) and (EC:2.1.3.6)] that convert spermidine to putrescine. Polyamines are among the uremic toxins which accelerate progression of uremia [71, 72]. Polyamines originate from L-ornithine and methionine by ornithine decarboxylase (EC 4.1.1.17). Decarboxylation of L-ornithine leads to the production of putrescine which is further converted to higher polyamines spermidine and spermine by successive addition of aminopropyl groups derived from decarboxylated S-adenosylmethionine. These metabolites which are linked with CCr correlated with specific gut microbiota. Microbiota-derived polyamine metabolites exacerbate the damage of intestinal epithelial tight junction, which in turn accelerates the translocation of uremic toxins into the systemic circulation and promotes local and systemic inflammations [8].

Treatment of PAA and PC in CKD rats prevented the disruption of intestinal epithelial barrier by downregulating polyamine metabolites as well as upregulating ZO1, occludin and claudin-1 protein expression. In addition, it mitigated inflammation and oxidative stress by inhibiting IκBα/NF-κB pathway and maintaining Keap1/Nrf2 pathway as well, the dysregulation of which contributed much to renal fibrosis in the untreated CKD rats. Finally, PAA and PC treatment also improved CCr as well as lowered SBP, DBP, serum creatinine, urea concentrations, proteinuria, and downregulated α-SMA, vimentin and collagen I expression in CKD rats.

Our study further indicated that the elevated blood pressure was deeply implicated in glycine metabolism pathway. Glycine-conjugated metabolites including cinnamoylglycine, phenylpropionylglycine, 2-phenylacetic acid and hippuric acid showed strong positive or negative correlation with five genera in CKD rats. Although both the treatment of PAA and PC could alter metabolites derived from glycine and polyamine metabolism, PAA exhibited a stronger effect on lowering production of glycine-conjugated metabolites as well as the downregulation of α-SMA, vimentin and collagen I expressions in CKD rats. Taken together, these microbial genera and glycine-conjugated metabolites were intimately involved in renal injury and hypertension.

Conclusion

CKD significantly modified the structure and composition of gut bacteria in rats. The shifts in the composition of the gut bacteria, in turn, played an important role in the progression of CKD. In this study, we demonstrated the CKD-induced microbial dysbiosis and the dysregulation of microbial metabolites as well as their impact on renal fibrosis and renal impairment. Additionally, we further showed that treatment with PAA and PC mitigated microbial dysbiosis, attenuated oxidative stress, inflammation and renal fibrosis, and retarded the decline of renal function in rats with CKD induced by 5/6 nephrectomy.

Acknowledgements This study was supported by the National Natural Science Foundation of China (nos. 81872985, 81673578, 81603271).

Compliance with ethical standards

Conflict of interest The authors declare that they have no competing interests.

References

1. Webster AC, Nagler EV, Morton RL, Masson P (2017) Chronic kidney disease. Lancet 389:1238–1252
2. Schmidt M, Mansfield KE, Bhaskaran K, Nitsch D, Sorensen HT, Smeeth L, Tomlinson LA (2017) Serum creatinine elevation after renin-angiotensin system blockade and long term cardiorenal risks: cohort study. BMJ 356:j791
3. Pickard JM, Zeng MY, Caruso R, Nunez G (2017) Gut microbiota: role in pathogen colonization, immune responses, and inflammatory disease. Immunol Rev 279:70–89
4. Schroeder BO, Backhed F (2016) Signals from the gut microbiota to distant organs in physiology and disease. Nat Med 22:1079–1089
5. Rooks MG, Garrett WS (2016) Gut microbiota, metabolites and host immunity. Nat Rev Immunol 16:341–352
6. Vaziri ND, Zhao YY, Pahl MV (2016) Altered intestinal microbial flora and impaired epithelial barrier structure and function in CKD: the nature, mechanisms, consequences and potential treatment. Nephrol Dial Transplant 31:737–746
7. Coppo R (2018) The gut-kidney axis in IgA nephropathy: role of microbiota and diet on genetic predisposition. Pediatr Nephrol 33:53–61
8. Chen YY, Chen DQ, Chen L, Liu JR, Vaziri ND, Guo Y, Zhao YY (2019) Microbiome-metabolome reveals the contribution of gut-kidney axis on kidney disease. J Transl Med 17:5
9. Vaziri ND, Wong J, Pahl M, Piceno YM, Yuan J, DeSantis TZ, Ni Z, Nguyen TH, Andersen GL (2013) Chronic kidney disease alters intestinal microbial flora. Kidney Int 83:308–315
10. Simoes-Silva L, Araujo R, Pestana M, Soares-Silva I, Sampaio-Maia B (2018) The microbiome in chronic kidney disease patients undergoing hemodialysis and peritoneal dialysis. Pharmacol Res 130:143–151
11. Anders HJ, Andersen K, Stecher B (2013) The intestinal microbiota, a leaky gut, and abnormal immunity in kidney disease. Kidney Int 83:1010–1016
12. Vaziri ND (2012) CKD impairs barrier function and alters microbial flora of the intestine: a major link to inflammation and uremic toxicity. Curr Opin Nephrol Hypertens 21:587–592
13. Rossi M, Campbell KL, Johnson DW, Stanton T, Vesey DA, Coombes JS, Weston KS, Hawley CM, McWhinney BC, Ungerer JP, Isbel N (2014) Protein-bound uremic toxins, inflammation and oxidative stress: a cross-sectional study in stage 3-4 chronic kidney disease. Arch Med Res 45:309–317
14. Tang WH, Wang Z, Kennedy DJ, Wu Y, Buffa JA, Agatisa-Boyle B, Li XS, Levison BS, Hazen SL (2015) Gut microbiota-dependent trimethylamine N-oxide (TMAO) pathway contributes to both development of renal insufficiency and mortality risk in chronic kidney disease. Circ Res 116:448–455
15. Griffin KA, Picken M, Bidani AK (1994) Method of renal mass reduction is a critical modulator of subsequent hypertension and glomerular injury. J Am Soc Nephrol 4:2023–2031
16. Iyoda M, Shibata T, Hirai Y, Kuno Y, Akizawa T (2011) Nilotinib attenuates renal injury and prolongs survival in chronic kidney disease. J Am Soc Nephrol 22:1486–1496
17. Zhang ZH, Vaziri ND, Wei F, Cheng XL, Bai X, Zhao YY (2016) An integrated lipidomics and metabolomics reveal nephroprotective effect and biochemical mechanism of Rheum officinale in chronic renal failure. Sci Rep 6:22151
18. Zhang ZH, Wei F, Vaziri ND, Cheng XL, Bai X, Lin RC, Zhao YY (2015) Metabolomics insights into chronic kidney disease and modulatory effect of rhubarb against tubulointerstitial fibrosis. Sci Rep 5:14472
19. Wang M, Chen DQ, Chen L, Cao G, Zhao H, Liu D, Vaziri ND, Guo Y, Zhao YY (2018) Novel inhibitors of the cellular renin-angiotensin system components, poricoic acids, target Smad3 phosphorylation and Wnt/β-catenin pathway against renal fibrosis. Br J Pharmacol 175:2689–2708
20. Chen H, Yang T, Wang MC, Chen DQ, Yang Y, Zhao YY (2018) Novel RAS inhibitor 25-O-methylalisol F attenuates

epithelial-to-mesenchymal transition and tubulo-interstitial fibrosis by selectively inhibiting TGF-β-mediated Smad3 phosphorylation. Phytomedicine 42:207–218
21. Bolger A, Lohse M, Usadel B (2014) Trimmomatic: a flexible trimmer for Illumina sequence data. Bioinformatics 30:2114–2120
22. Edgar RC, Flyvbjerg H (2015) Error filtering, pair assembly and error correction for next-generation sequencing reads. Bioinformatics 31:3476–3482
23. Edgar RC (2013) UPARSE: highly accurate OTU sequences from microbial amplicon reads. Nat Methods 10:996–998
24. Edgar R (2016) SINTAX: a simple non-Bayesian taxonomy classifier for 16S and ITS sequences. bioRxiv 074161. https://doi.org/10.1101/074161
25. Edgar RC (2010) Search and clustering orders of magnitude faster than BLAST. Bioinformatics 26:2460–2461
26. Lozupone C, Knight R (2005) UniFrac: a new phylogenetic method for comparing microbial communities. Appl Environ Microbiol 71:8228–8235
27. Caporaso JG, Kuczynski J, Stombaugh J, Bittinger K, Bushman FD, Costello EK, Fierer N, Peña AG, Goodrich JK, Gordon JI (2010) QIIME allows analysis of high-throughput community sequencing data. Nat Methods 7:335–336
28. Chen DQ, Cao G, Chen H, Argyopoulos CP, Yu H, Su W, Chen L, Samuels DC, Zhuang S, Bayliss GP, Zhao S, Yu XY, Vaziri ND, Wang M, Liu D, Mao JR, Ma SX, Zhao J, Zhang Y, Shang YQ, Kang H, Ye F, Cheng XH, Li XR, Zhang L, Meng MX, Guo Y, Zhao YY (2019) Identification of serum metabolites associating with chronic kidney disease progression and anti-fibrotic effect of 5-methoxytryptophan. Nat Commun 10:1476
29. Chen DQ, Cao G, Chen H, Liu D, Su W, Yu XY, Vaziri ND, Liu XH, Bai X, Zhang L, Zhao YY (2017) Gene and protein expressions and metabolomics exhibit activated redox signaling and Wnt/β-catenin pathway are associated with metabolite dysfunction in patients with chronic kidney disease. Redox Biol 12:505–521
30. Zhang ZH, Chen H, Vaziri ND, Mao JR, Zhang L, Bai X, Zhao YY (2016) Metabolomic signatures of chronic kidney disease of diverse etiologies in the rats and humans. J Proteome Res 15:3802–3812
31. Zhao YY, Cheng XL, Wei F, Xiao XY, Sun WJ, Zhang Y, Lin RC (2012) Serum metabonomics study of adenine-induced chronic renal failure in rats by ultra performance liquid chromatography coupled with quadrupole time-of-flight mass spectrometry. Biomarkers 17:48–55
32. Kikuchi M, Ueno M, Itoh Y, Suda W, Hattori M (2017) Uremic toxin-producing gut microbiota in rats with chronic kidney disease. Nephron 135:51–60
33. Meyer TW, Hostetter TH (2012) Uremic solutes from colon microbes. Kidney Int 81:949–954
34. Zeisel SH, Warrier M (2017) Trimethylamine N-oxide, the microbiome, and heart and kidney disease. Annu Rev Nutr 37:157–181
35. Zhao YY, Liu J, Cheng XL, Bai X, Lin RC (2012) Urinary metabonomics study on biochemical changes in an experimental model of chronic renal failure by adenine based on UPLC Q-TOF/MS. Clin Chim Acta 413:642–649
36. Zhao YY, Cheng XL, Wei F, Bai X, Tan XJ, Lin RC, Mei Q (2013) Intrarenal metabolomic investigation of chronic kidney disease and its TGF-β1 mechanism in induced-adenine rats using UPLC Q-TOF/HSMS/MS^{E}. J Proteome Res 12:2692–2703
37. Zhao YY, Cheng XL, Wei F, Bai X, Lin RC (2012) Application of faecal metabonomics on an experimental model of tubulointerstitial fibrosis by ultra performance liquid chromatography/high-sensitivity mass spectrometry with MS^{E} data collection technique. Biomarkers 17:721–729
38. Li Y, Sekula P, Wuttke M, Wahrheit J, Hausknecht B, Schultheiss UT, Gronwald W, Schlosser P, Tucci S, Ekici AB, Spiekerkoetter U, Kronenberg F, Eckardt KU, Oefner PJ, Kottgen A (2018) Genome-wide association studies of metabolites in patients with CKD identify multiple loci and illuminate tubular transport mechanisms. J Am Soc Nephrol 29:1513–1524
39. Zhao YY, Feng YL, Du X, Xi ZH, Cheng XL, Wei F (2012) Diuretic activity of the ethanol and aqueous extracts of the surface layer of *Poria cocos* in rat. J Ethnopharmacol 144:775–778
40. Feng YL, Lei P, Tian T, Yin L, Chen DQ, Chen H, Mei Q, Zhao YY, Lin RC (2013) Diuretic activity of some fractions of the epidermis of *Poria cocos*. J Ethnopharmacol 150:1114–1118
41. Chen L, Cao G, Wang M, Feng YL, Chen DQ, Vaziri ND, Zhuang S, Zhao YY (2019) The matrix metalloproteinase-13 Inhibitor poricoic acid ZI ameliorates renal fibrosis by mitigating epithelial-mesenchymal transition. Mol Nutr Food Res 63:1900132
42. Zhao YY, Feng YL, Bai X, Tan XJ, Lin RC, Mei Q (2013) Ultra performance liquid chromatography-based metabonomic study of therapeutic effect of the surface layer of *Poria cocos* on adenine-induced chronic kidney disease provides new insight into anti-fibrosis mechanism. PLoS One 8:e59617
43. Zhao YY, Li HT, Feng YI, Bai X, Lin RC (2013) Urinary metabonomic study of the surface layer of *Poria cocos* as an effective treatment for chronic renal injury in rats. J Ethnopharmacol 148:403–410
44. Zhao YY, Lei P, Chen DQ, Feng YL, Bai X (2013) Renal metabolic profiling of early renal injury and renoprotective effects of *Poria cocos* epidermis using UPLC Q-TOF/HSMS/MSE. J Pharm Biomed Anal 81–82:202–209
45. Miao H, Zhao YH, Vaziri ND, Tang DD, Chen H, Chen H, Khazaeli M, Tarbiat-Boldaji M, Hatami L, Zhao YY (2016) Lipidomics biomarkers of diet-induced hyperlipidemia and Its treatment with *Poria cocos*. J Agric Food Chem 64:969–979
46. Chen DQ, Feng YL, Chen L, Liu JR, Wang M, Vaziri ND, Zhao YY (2019) Poricoic acid A enhances melatonin inhibition of AKI-to-CKD transition by regulating Gas6/Axl-NF-κB/Nrf2 axis. Free Radic Biol Med 134:484–497
47. Wang M, Chen DQ, Wang MC, Chen H, Chen L, Liu D, Zhao H, Zhao YY (2017) Poricoic acid ZA, a novel RAS inhibitor, attenuates tubulo-interstitial fibrosis and podocyte injury by inhibiting TGF-β/Smad signaling pathway. Phytomedicine 36:243–253
48. Wang M, Chen DQ, Chen L, Zhao H, Liu D, Zhang ZH, Vaziri ND, Guo Y, Zhao YY, Cao G (2018) Novel RAS inhibitors poricoic acid ZG and poricoic acid ZH attenuate renal fibrosis via Wnt/β-catenin pathway and targeted phosphorylation of smad3 signaling. J Agric Food Chem 66:1828–1842
49. Yang T, Richards EM, Pepine CJ, Raizada MK (2018) The gut microbiota and the brain-gut-kidney axis in hypertension and chronic kidney disease. Nat Rev Nephrol 14:442–456
50. Chen H, Cao G, Chen DQ, Wang M, Vaziri ND, Zhang ZH, Mao JR, Bai X, Zhao YY (2016) Metabolomics insights into activated redox signaling and lipid metabolism dysfunction in chronic kidney disease progression. Redox Biol 10:168–178
51. Chen DQ, Chen H, Chen L, Vaziri ND, Wang M, Li XR, Zhao YY (2017) The link between phenotype and fatty acid metabolism in advanced chronic kidney disease. Nephrol Dial Transplant 32:1154–1166
52. Kieffer DA, Piccolo BD, Vaziri ND, Liu S, Lau WL, Khazaeli M, Nazertehrani S, Moore ME, Marco ML, Martin RJ, Adams SH (2016) Resistant starch alters gut microbiome and metabolomic profiles concurrent with amelioration of chronic kidney disease in rats. Am J Physiol Renal Physiol 310:F857–F871
53. Vaziri ND, Liu SM, Lau WL, Khazaeli M, Nazertehrani S, Farzaneh SH, Kieffer DA, Adams SH, Martin RJ (2014) High amylose resistant starch diet ameliorates oxidative stress, inflammation, and progression of chronic kidney disease. PLoS One 9:e114881
54. Wang F, Jiang H, Shi K, Ren Y, Zhang P, Cheng S (2012) Gut bacterial translocation is associated with microinflammation in end-stage renal disease patients. Nephrology 17:733–738

55. Gaastra W, Kusters JG, van Duijkeren E, Lipman LJ (2014) *Escherichia fergusonii*. Vet Microbiol 172:7–12
56. Oh JY, Kang MS, An BK, Shin EG, Kim MJ, Kwon JH, Kwon YK (2012) Isolation and epidemiological characterization of heat-labile enterotoxin-producing *Escherichia fergusonii* from healthy chickens. Vet Microbiol 160:170–175
57. Hida M, Aiba Y, Sawamura S, Suzuki N, Satoh T, Koga Y (1996) Inhibition of the accumulation of uremic toxins in the blood and their precursors in the feces after oral administration of Lebenin, a lactic acid bacteria preparation, to uremic patients undergoing hemodialysis. Nephron 74:349–355
58. Zeng YQ, Dai Z, Lu F, Lu Z, Liu X, Chen C, Qu P, Li D, Hua Z, Qu Y, Zou C (2016) Emodin via colonic irrigation modulates gut microbiota and reduces uremic toxins in rats with chronic kidney disease. Oncotarget 7:17468–17478
59. Barrios C, Beaumont M, Pallister T, Villar J, Goodrich JK, Clark A, Pascual J, Ley RE, Spector TD, Bell JT, Menni C (2015) Gut-microbiota-metabolite axis in early renal function decline. PLoS One 10:e0134311
60. Nazzal L, Roberts J, Singh P, Jhawar S, Matalon A, Gao Z, Holzman R, Liebes L, Blaser MJ, Lowenstein J (2017) Microbiome perturbation by oral vancomycin reduces plasma concentration of two gut-derived uremic solutes, indoxyl sulfate and p-cresyl sulfate, in end-stage renal disease. Nephrol Dial Transplant 32:1809–1817
61. Mishima E, Fukuda S, Shima H, Hirayama A, Akiyama Y, Takeuchi Y, Fukuda NN, Suzuki T, Suzuki C, Yuri A, Kikuchi K, Tomioka Y, Ito S, Soga T, Abe T (2015) Alteration of the intestinal environment by lubiprostone is associated with amelioration of adenine-induced CKD. J Am Soc Nephrol 26:1787–1794
62. Xu KY, Xia GH, Lu JQ, Chen MX, Zhen X, Wang S, You C, Nie J, Zhou HW, Yin J (2017) Impaired renal function and dysbiosis of gut microbiota contribute to increased trimethylamine-N-oxide in chronic kidney disease patients. Sci Rep 7:1445
63. Jiang S, Xie S, Lv D, Wang P, He H, Zhang T, Zhou Y, Lin Q, Zhou H, Jiang J, Nie J, Hou F, Chen Y (2017) Alteration of the gut microbiota in Chinese population with chronic kidney disease. Sci Rep 7:2870
64. Stern JM, Moazami S, Qiu Y, Kurland I, Chen Z, Agalliu I, Burk R, Davies KP (2016) Evidence for a distinct gut microbiome in kidney stone formers compared to non-stone formers. Urolithiasis 44:399–407
65. Santisteban MM, Qi Y, Zubcevic J, Kim S, Yang T, Shenoy V, Cole-Jeffrey CT, Lobaton GO, Stewart DC, Rubiano A, Simmons CS, Garcia-Pereira F, Johnson RD, Pepine CJ, Raizada MK (2017) Hypertension-linked pathophysiological alterations in the gut. Circ Res 120:312–323
66. Pryde SE, Duncan SH, Hold GL, Stewart CS, Flint HJ (2002) The microbiology of butyrate formation in the human colon. FEMS Microbiol Lett 217:133–139
67. Li YN, Huang F, Cheng HJ, Li SY, Liu L, Wang LY (2014) Intestine-derived *Clostridium leptum* induces murine tolerogenic dendritic cells and regulatory T cells in vitro. Hum Immunol 75:1232–1238
68. Besouw M, Cornelissen E, Cassiman D, Kluijtmans L, van den Heuvel L, Levtchenko E (2014) Carnitine profile and effect of suppletion in children with renal fanconi syndrome due to cystinosis. JIMD Rep 16:25–30
69. Araujo MV, Hong BY, Fava PL, Khan S, Burleson JA, Fares G, Samson W, Strausbaugh LD, Diaz PI, Ioannidou E (2015) End stage renal disease as a modifier of the periodontal microbiome. BMC Nephrol 16:80
70. Tain YL, Lee WC, Wu KLH, Leu S, Chan JYH (2018) Resveratrol prevents the development of hypertension programmed by maternal Plus post-weaning high-fructose consumption through modulation of oxidative stress, nutrient-sensing signals, and gut microbiota. Mol Nutr Food Res 62:e1800066
71. Sindhu KK (2016) Uremic toxins: some thoughts on acrolein and spermine. Ren Fail 38:1755–1758
72. Goek ON, Prehn C, Sekula P, Romisch-Margl W, Doring A, Gieger C, Heier M, Koenig W, Wang-Sattler R, Illig T, Suhre K, Adamski J, Kottgen A, Meisinger C (2013) Metabolites associate with kidney function decline and incident chronic kidney disease in the general population. Nephrol Dial Transplant 28:32131–32138